Active Control of Self-Induced Roll Oscillations of a Wing Using Synthetic Jet

Tianxiang Hu[1], Zhijin Wang[2], Ismet Gursul[3] and Chris R. Bowen[4]
University of Bath, Bath, BA2 7AY, United Kingdom
Email: i.a.gursul@bath.ac.uk
[1]Postgraduate Student, Department of Mechanical Engineering.
[2]Lecturer, Department of Mechanical Engineering, Member AIAA.
[3]Professor, Department of Mechanical Engineering, Associate Fellow AIAA.
[4]Professor, Department of Mechanical Engineering.

Received date 12/9/2013; Accepted date 18/12/2013

ABSTRACT

Active control of self-excited roll oscillations of a rectangular flat plate wing with an aspect ratio of two was studied experimentally in a wind tunnel, using synthetic jet excitation near the leading edge. It was found that, by activating the synthetic jet excitation at an optimum frequency of $St = 1$, large amplitude roll oscillations could be attenuated and the onset of the oscillation can be delayed by up to $\Delta\alpha_{max} = 3.5°$ for extremely small values of momentum coefficient. High frame-rate Particle Image Velocimetry (PIV) measurements revealed a strong resonance between the synthetic jet excitation and shear layer instabilities. The resonance energizes the shear layer separated from the leading edge and results in a local flow field that is more typical of lower wing incidence, thus effectively suppressing roll oscillations.

1. INTRODUCTION

In the past decade, Micro Air Vehicles (MAVs) have received growing interest in various areas of research because of their broad range of applications. MAVs with fixed low-aspect-ratio (LAR) wings have operating speeds around 10 m/s with dimensions between 10 and 15 cm. The aerodynamics of LAR wings with various airfoil and planform shapes at low Reynolds numbers have been studied previously [1, 2].

Recent flight tests of a variety of designs of MAVs unveiled the onset of unwanted large amplitude roll oscillations, which eventually resulted in difficulties with flight control [3]. Roll instabilities and oscillations are inherent to the fixed-wing MAV configurations due to their low aspect ratio wings and low mass moment of inertia I_{xx} [4]. Undesired limited-cycle roll oscillations are often referred to as "wing rock", which was first observed on free-to-roll slender delta wings [5, 6]. These roll oscillations were well studied and recognized as the fluid-structure interaction between the leading-edge vortices and the wing body. Similar fluid-structure interactions resulting in wing roll oscillations were also reported in later studies of LAR ($AR \leq 0.5$) rectangular wings [7, 8].

Recent studies carried out at the University of Bath to investigate the free-to-roll non-slender delta wings found that self-induced roll oscillations also occurred for delta wings with sweep angle $\Lambda \leq 60°$ but with a non-zero mean roll angle around the stall angle of attack [9, 10]. More recently, experimental investigations were carried out on relatively higher aspect ratio ($AR = 2$ and 4) free-to-roll rectangular flat plate wings. The results showed that, even at pre-stall incidences, self-excited roll oscillations occur [11, 12]. Velocity measurements suggested that the onset of these self-induced roll oscillations was closely related to the loss of reattachment of the leading-edge separation bubble. Therefore it might be an effective approach to suppress self-induced roll oscillations by restoring partial flow reattachment over the suction surface using appropriate flow control techniques.

---

[1]Postgraduate Student, Department of Mechanical Engineering.

[2]Lecturer, Department of Mechanical Engineering, Member AIAA.

[3]Professor, Department of Mechanical Engineering, Associate Fellow AIAA.

[4]Professor, Department of Mechanical Engineering.

Both passive [13] and active [14–17] flow control techniques have been applied to suppress self-induced roll oscillations of slender delta wings. Katz [6] reviewed all the techniques and concluded that active techniques are more effective in the attenuation of wing rock. More recently, acoustic forcing was applied to suppress the roll oscillation of rectangular wings (AR = 2) of various airfoil profiles [18,19]. It was found that the onset of self-induced roll oscillations of a flat plate wing can be delayed up to $\Delta\alpha_{max} \approx 4°$ and the magnitude of oscillations can be suppressed up to $\Delta\Phi_{rms,max} \approx 30°$ by using acoustic forcing at an optimized excitation frequency of St = 1.5 ($St = fc/U_\infty$, where f is the excitation frequency, c is the root-chord length and U_∞ is the freestream velocity). Similar results were also observed for rectangular wings with NACA0012 and SD7003-085-88 airfoil profiles. High frame-rate particle image velocimetry (PIV) measurements illustrated resonance between the acoustic forcing at optimized frequencies and leading-edge shear layer instabilities. The resonance energized the shear layer separated from the leading edge and promoted partial reattachment, which in turn attenuated the self-induced roll oscillations. These investigations demonstrated the potential of acoustic forcing using a speaker in increasing the robustness of MAVs to atmospheric disturbances. However, in practice it is difficult to place such a speaker on a MAV. Furthermore, acoustic forcing is a global flow control technique, whereas a local excitation scheme might be more effective. This is the motivation of the present study.

Synthetic jets have been used as effective actuators [20] in active flow control applications for separation control to delay stall and increase lift [21–24], thrust enhancement [25], and tip-vortex control [26]. In the present research, synthetic jet blowing was employed to attenuate self-induced roll oscillations of a LAR rectangular wing. In contrast to previous acoustic excitation studies, synthetic jet excitation was applied near the leading-edge of a LAR flat-plate wing only. Its effectiveness in suppressing self-excited roll oscillations was investigated in wind tunnel experiments. Particle image velocimetry measurements were conducted to understand the underlying flow physics.

Another challenge of flow control for MAVs is that, for fixed-wing configurations, thin cross-sections are generally preferable at low Reynolds numbers [27]. Hence, placing synthetic jet actuators and blowing chambers is difficult as the space is insufficient due to the thin cross-sections. In the present study, an adaptation of synthetic jet actuator has been used to accommodate the thin cross-section of the flat-plate wing. Alternatively, actuators that do not need blowing chambers may be considered. For example, plasma actuators may have advantages. However, when the power supply is considered, they may not be practical at these small scales.

2. EXPERIMENTAL APPARATUS AND METHODS

2.1. Closed-loop wind tunnel

The experiments were conducted in a closed-loop wind tunnel located at the Department of Mechanical Engineering of the University of Bath. The test section of the wind tunnel has dimensions of 2.13 × 1.52 × 2.70 m. The tunnel can be operated at speeds of up to 50 m/s with a turbulence level of less than 0.1%. The experimental arrangement and layout of the working section are shown in Figure 1. The wing model and free-to-roll device are mounted on the high-alpha rig that allows the angle of attack to be varied with an accuracy of ±0.25 degrees as the wind tunnel is running.

2.2. Free-to-roll (FTR) device

The free-to-roll device consists of a shaft that is supported in greased bearings, so is free to rotate with minimal friction. One end of the shaft is attached to a potentiometer which outputs a varying voltage, linearly dependent on the roll angle Φ, while the other end of the shaft is attached to the sting upon which the wing is supported (Figure 1). The output from the potentiometer was fed to the computer via an A-D converter at a sampling frequency of 200 Hz for 120 seconds over a range of angles of attack with an estimated uncertainty of ±1°. Time history of roll oscillations were recorded, and then the maximum, mean, minimum and root-mean-square (RMS) roll angles for the recorded time period were calculated. The sting used for attaching the wing model to the free-to-roll device was in line with the roll axis of the wing as shown in Figure 2(a), hence there was no coning motion, just pure roll.

2.3. Flat plate wing model and synthetic jet

A rectangular flat plate wing with an aspect ratio of AR = 2 and a chord length of 167.5 mm was tested. The model was made of 3 mm thick aluminium plate with round edges (semi-circular shape). The sting

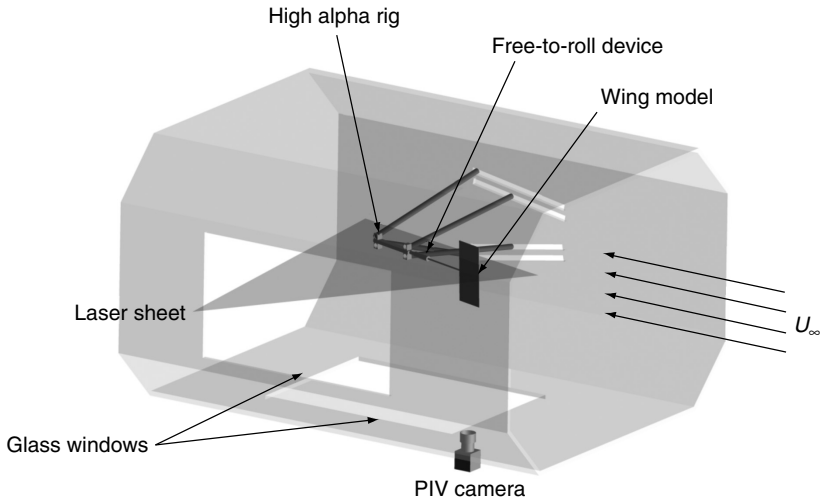

Figure 1. Schematic of the experimental setup.

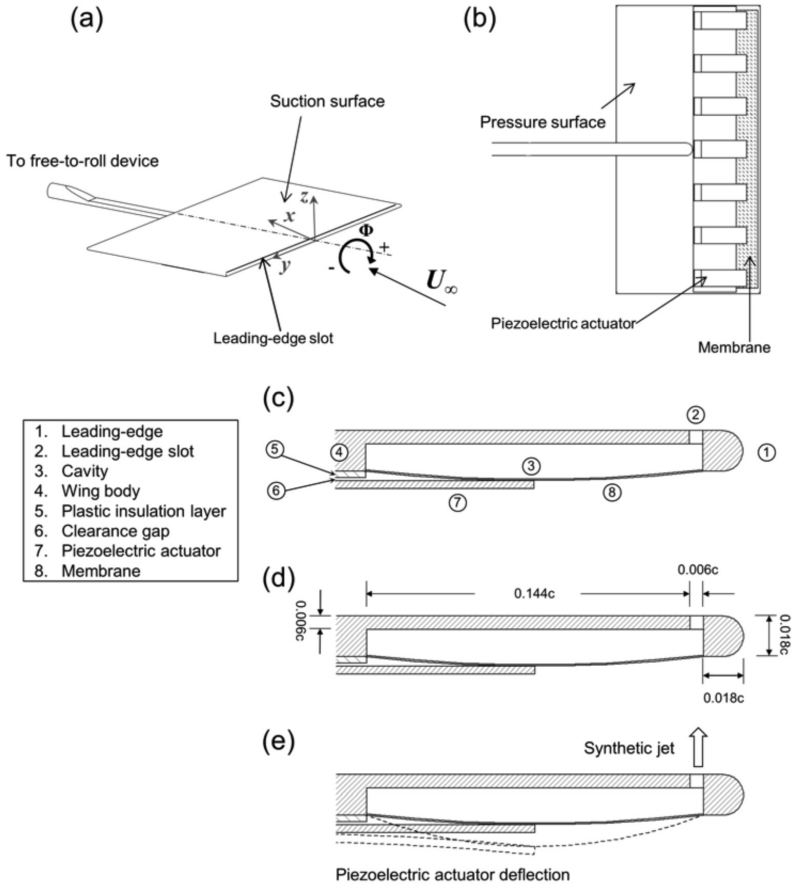

Figure 2. (a) Flat-plate wing with synthetic jet near leading-edge; (b) pressure surface; (c) cross-sectional view of leading-edge; (d) main dimensions; (e) concept of synthetic jet actuation.

was attached to the pressure surface of the model, resulting in a suction surface with no protrusions, as shown in Figures 2a&b. The physical properties of the wing model are shown in Table 1. The maximum blockage was approximately 2.3%. The models were painted matt black in order to reduce reflections created from the laser sheet during the PIV tests. The moment of inertia about the roll axis was

Table 1. Properties of wing model and piezoelectric actuators.

Wing model profile	**Flat plate**	**Piezoelectric actuator**	**APCI 40–2010**
Chord length c	167.5 mm	Length	60 mm
Aspect ratio AR	2	Free Length	53 mm
Thickness d	3 mm	Width	20 mm
Leading-edge profile	round (semicircle)	Thickness	0.6 mm
Side-edge profile	round (semicircle)	Resonance Frequency	65 Hz
Material	aluminium	Maximum deflection	2.5 mm
Weight	0.461 kg	Blocking Force	0.25 N
Moment of inertia I_{xx}	0.00435 kg m^2	Capacitance	1.7×10^5 μF

calculated using CAD software, which was calibrated using the measured mass of the wing, and included the moment of inertia of the sting used. The moment of inertia determines the frequency of the roll oscillations for the no-excitation case. For the present wing, the Strouhal number for the reference case is $St = 0.0089$, which is much smaller than that of the excitation frequency. Experiments were conducted at a free stream velocity of $U_\infty = 10$ m/s ($Re = 1.14 \times 10^5$ based on wing root chord length).

The synthetic jet was generated from periodic excitation of a cavity using a diaphragm oscillated by bilaminar flexing piezoelectric actuators (APC International, Ltd., APCI 40-2010) (Figure 2b; Table 1). The synthetic jet blowing was applied through the slot with a width of 1 mm (0.006c) along the leading-edge (Figure 2c-e). The membrane is 0.2 mm thick with Young's Modulus of $E = 2.2$ MPa and density of $\rho_m = 1$ gr/cm^3. For the purpose of achieving a uniform jet flow along the leading-edge, seven piezoelectric actuators were used on the pressure surface (Figures 2b and 2c). The distance between the centerlines of two neighbouring actuators was 50 mm. There was a clearance gap of 0.2 mm between the actuators and the insulation layer (Figure 2c). Therefore, the actuators could be operated without touching the wing body, thus maximizing the effective deflection of the actuators.

In the present study, the piezoelectric actuators were driven at a constant input voltage of 150 V by using a power supply (Bremi BRS33) and a function generator (Feedback PFG605). This approach of keeping constant excitation voltage will be justified below. The resonant frequency of the first bending mode of the actuators was measured as $f \approx 65$ Hz from its electro-mechanical resonance using a Solatron 1260 frequency response analyser. Experiments were conducted over an actuation frequency range of $f = 35 - 90$ Hz (corresponding to $St = fc/U_\infty = 0.59 - 1.5$). The jet velocity U_j was measured by a TSI 1210 hotwire probe in the absence of freestream. The hotwire probe was located along the centreline of the slot and 1 mm above the wing suction surface. The sampling frequency was 2 kHz. The momentum coefficient C_μ of synthetic jet blowing was estimated as $C_\mu = \dfrac{\rho \overline{U_{jet}}^2 wl}{q_\infty cb}$. Here U_{jet} is the instantaneous jet velocity, w is the slot width, l is the slot length, $q\infty$ is freestream dynamic pressure, c is the wing root-chord length, and b is the wing span. Given the dimension of the slot width and location of velocity measurements, we assume a uniform velocity magnitude across the slot width in the calculation of the momentum coefficient.

2.4. Particle Image Velocimetry (PIV) system

Quantitative flow measurements in the streamwise planes at various spanwise locations over the stationary wing were undertaken using a TSI high frame-rate PIV system. Illumination of desired plane was achieved using a New Wave Pegasus Nd:YLF double pulse high speed laser with a maximum energy of 10 mJ per pulse. The laser sheet was placed parallel to the freestream velocity. The images were captured using a TSI PowerView HS-3000 high speed CMOS camera with the resolution of 1024 × 1024 pixels. A TSI LaserPulse synchroniser unit was utilized to link the camera and the laser to enable the accurate capture for two frame cross-correlation analysis. The flow was seeded with olive oil droplets produced by a TSI model 9307-6 multi-jet atomizer. The mean size of the olive oil droplets was about 1 μm. The system was operated at sampling frequency

of 2 kHz, which allowed a capturing rate of 1 kHz for velocity field measurements and 6000 instantaneous images were captured for each measurement plane. The images were analysed using the Insight 3G software with a FFT cross-correlation algorithm and a Gussian peak engine to obtain the velocity vectors. The interrogation window size was 16 by 16 pixels and the effective grid size was around 1 mm. Various sources of uncertainty, including correlation errors, level of seeding, misalignment of the PIV setup, and out-of-plane motion of the seeding particles may contribute. Taking all these aspects into consideration, the measurement uncertainty for velocity was estimated as 2%.

3. RESULTS AND DISCUSSION

3.1. Synthetic jet

Figure 3 shows the time history of the hotwire measurements of the synthetic jet velocity at the centreline of the slot and 1 mm away from the suction surface with piezoelectric actuator input frequency of $f = 60$ Hz ($St = 1$). It can be observed that the synthetic jet velocity exhibits clear periodic pattern with a maximum peak-to-peak amplitude of 1.3 m/s ($0.13U_\infty$). Note that the non-zero time-averaged velocity is due to the entrainment effect since the hotwire measurement location was 1 mm away from the wing surface. The frequency spectra calculated from the time history of U_{jet} exhibits a dominant peak at the piezoelectric actuation frequency $f = 60$ Hz (not shown here) and very small peaks at higher harmonics.

The resonant frequency of piezoelectric actuators was $f = 65$ Hz ($St \approx 1.1$) and the experiments were conducted over the actuation frequency range of $f = 35 - 90$ Hz ($St = 0.59 - 1.5$) for a constant input voltage of 150 V. Figure 4 presents the time-averaged momentum coefficient of the synthetic jet blowing with a constant actuation input of 150 V as a function of excitation frequency. It can be observed that, for all the excitation frequencies tested, C_μ exhibits relatively small variations. Given that there is relatively large uncertainty in the calculation of the momentum coefficient, the actuation input was kept constant at 150 V in the present investigation, which simplified the experimental procedure significantly.

The shape of the curve in Figure 4 can be qualitatively understood. At around the resonant frequency ($St \approx 1.1$), the displacement is a maximum and is expected to decay at higher frequencies for a damped system. However, synthetic jet blowing velocity U_{jet} can be assumed to be proportional to the actuator velocity. Jet blowing velocity is therefore proportional to both actuation amplitude and actuation frequency. It appears that decreasing amplitude with increasing frequency results in relatively flat curve in Figure 4.

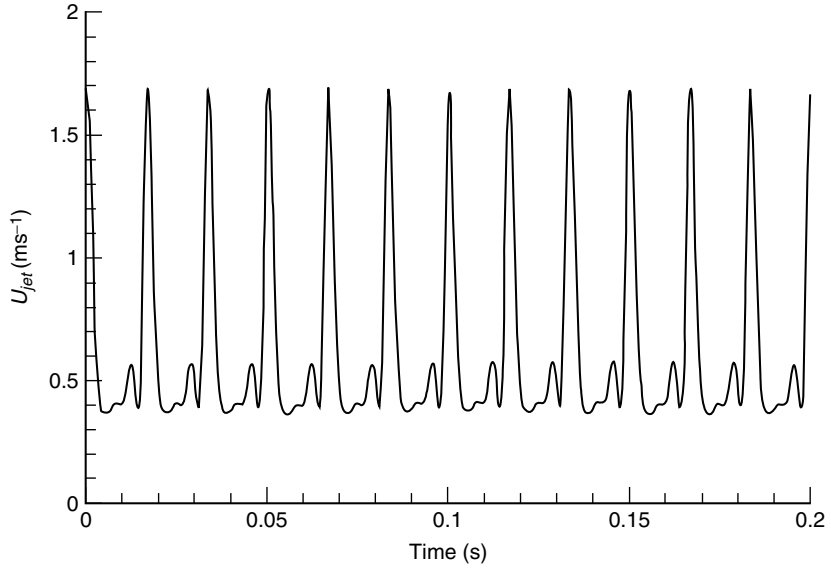

Figure 3. Time history of synthetic jet velocity measured at the centre of the slot and 1 mm away from the suction surface.

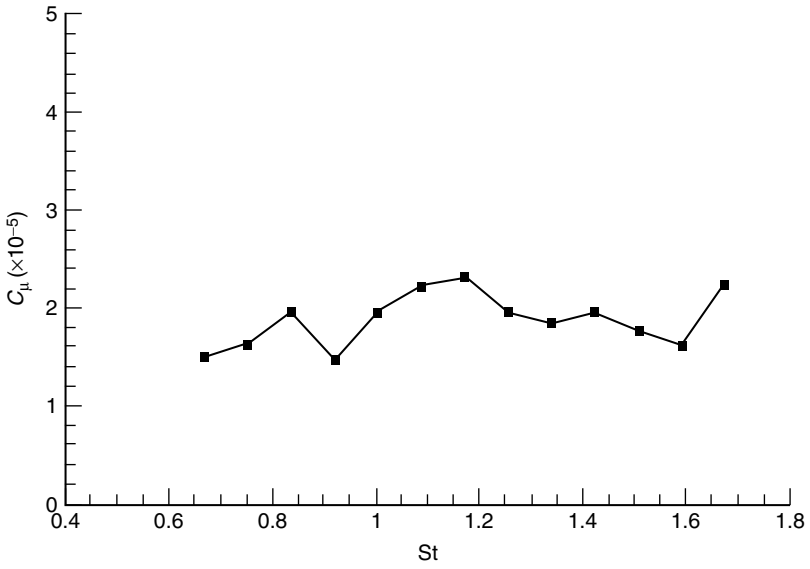

Figure 4. Time-averaged momentum coefficient of the synthetic jet as a function of excitation frequency.

It is also important to note that the estimated momentum coefficients are very small. It will be shown below that such small excitation levels are sufficient to supress large amplitude roll oscillations.

3.2. Attenuation of self-induced roll oscillations

The variations of mean, minimum and maximum roll angles of the self-excited roll oscillations with angle of attack of the flat-plate wing without and with synthetic jet excitation at $St = 1$ are presented in

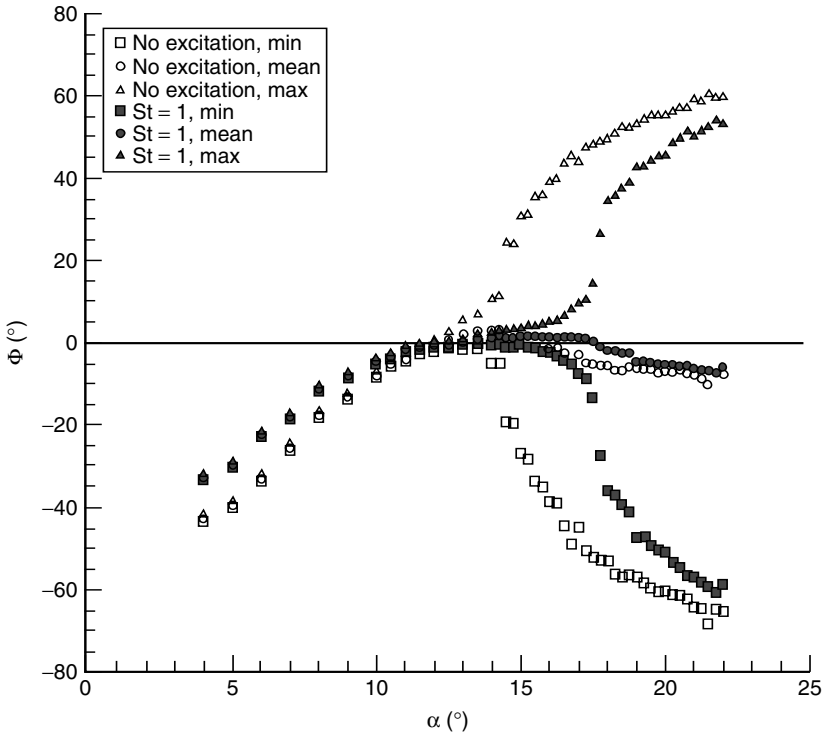

Figure 5. Variation of roll angle with angle of attack without and with synthetic jet excitation at $St = 1$.

Figure 5. It can be observed that, when there was no synthetic jet excitation, nonzero mean roll angle occurred at $\alpha \leq 11.5°$. Previous studies suggested that asymmetric leading-edge bubbles and therefore asymmetric tip vortices were possible at low incidences which result in nonzero mean roll angles [12, 18, 19]. When the wing incidence was increased to $\alpha = 13°$, small amplitude roll oscillations occurred due to the loss of reattachment of the leading-edge separation bubble [12]. For $\alpha \geq 14°$, a sharp increase in the amplitude of the wing roll oscillations occurred. For $\alpha \geq 17°$, the amplitude of the wing roll oscillations increased gradually with the angle of attack of the wing. Note that the mean roll angle remained close to zero degrees for $\alpha \geq 12°$.

Previous studies indicated that aforementioned large amplitude roll oscillations are accompanied by large scale separation from the leading-edge [12]. Effective flow excitation can energize the shear layer separated from the leading-edge and result in local reattachment or smaller separation regions, thus attenuating the roll oscillations [19]. In the present investigation, when a synthetic jet excitation at $St = 1$ was applied near the leading edge, the onset of the self-excited roll oscillation was delayed by approximately 3.5° of wing angle of attack to about 16°, followed by a sharp increase in the amplitude of the wing roll oscillations at about $\alpha = 17°$ (Figure 5). At $\alpha \geq 20°$, the amplitude of the wing roll oscillations increased gradually with increasing angle of attack and approached the values of the experiments without synthetic jet excitation. The synthetic jet excitation had little effect on the mean roll angle for $\alpha \geq 12°$.

The time histories of the wing roll angle without and with synthetic jet blowing near the leading edge at $\alpha = 17°$· are presented in Figure 6. It is seen that, when the synthetic jet was not activated, periodic roll oscillations occurred with an amplitude of about 40°. These large amplitude roll oscillations were however effectively suppressed to a few degrees by activating synthetic jet excitation at $St = 1$. Previous studies suggested that the effectiveness of excitation in attenuating and delaying roll oscillations is highly dependent on the excitation frequency [18, 19]. Figure 7a presents the root-mean-square (RMS) value of wing roll angle as a function of angle of attack without and with synthetic jet excitation at various frequencies. The reduction of RMS value of wing roll angle as a function of angle of attack with various synthetic jet excitation frequencies is presented in Figure 7b. It is seen from Figure 7a that, for all St tested, the synthetic jet excitation had no effect on the RMS values of the roll angle for $\alpha \leq 12°$. For $12° < \alpha < 21°$, however, the

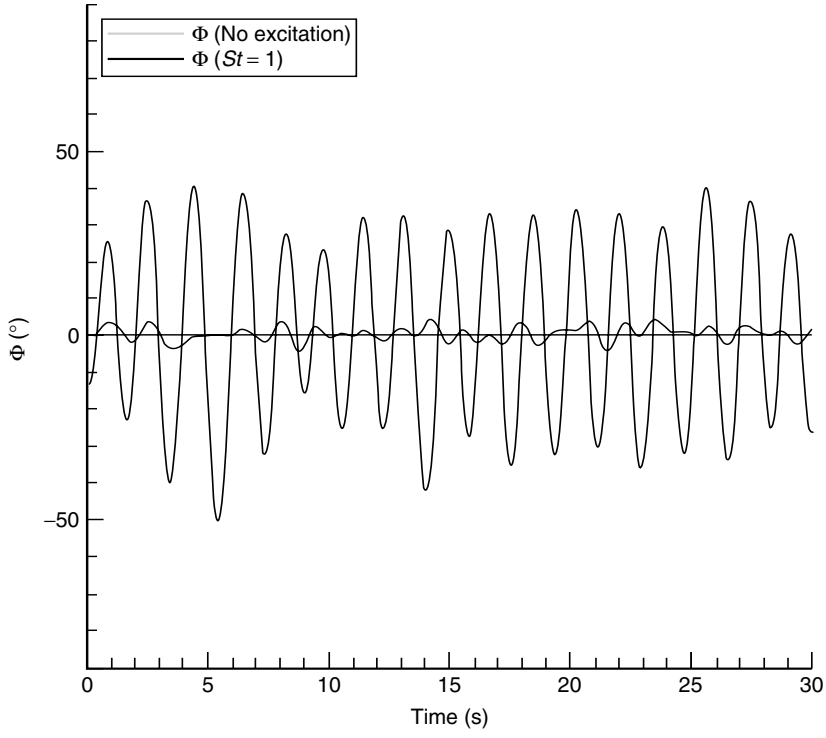

Figure 6. Time histories of the wing roll angle at $\alpha = 17°$ without and with synthetic jet excitation at $St = 1$.

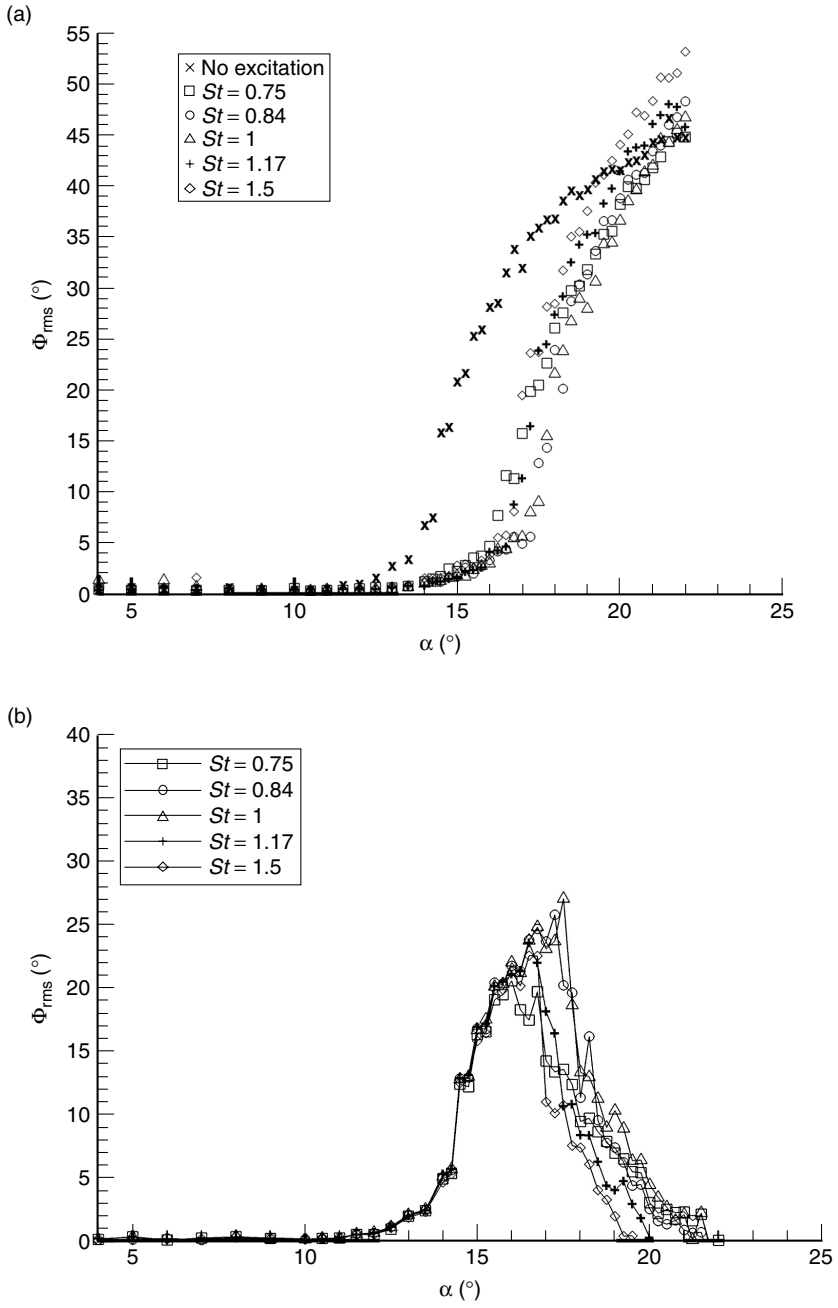

Figure 7. (a) RMS values of wing roll angle as a function of angle of attack without and with synthetic jet excitation in the range of $St = 0.75 - 1.5$; (b) Reduction of RMS values of wing roll angle as a function of angle of attack with various synthetic jet excitation frequencies of $St = 0.75 - 1.5$.

excitation suppressed the roll oscillations effectively. For $\alpha \geq 21°$, the amplitude of the wing roll oscillations approached the values of those from the experiments without synthetic jet excitation. Figure 7b also suggests that, for $12° \leq \alpha \leq 16°$, excitation at various frequencies exhibits similar effectiveness in supressing the roll oscillations. It is seen that, for $16° < \alpha \leq 21°$, the effectiveness of roll suppression increases with increasing Strouhal number for $0.75 \leq St \leq 1$. With further increase in Strouhal number ($St > 1$), the effectiveness of synthetic jet excitation decreased (Figure 7b). Figure 8a presents the RMS value of the roll angle as a function of Strouhal number of

the synthetic jet excitation for wing incidences between 15° and 19°, for which the effectiveness of excitation was significant. For all the values of angle of attack tested, a local minimum in RMS value of the roll angle is observed at around $St = 1$, suggesting that the optimum synthetic jet excitation frequency for attenuation of the roll oscillations corresponds to $St = 1$ for the flat plate wing.

When all angles of attack are considered, the maximum reduction, $\Delta\Phi_{rms,max}$ of RMS value of the wing roll angle is presented in Figure 8b as a function of Strouhal number of synthetic jet excitation. It

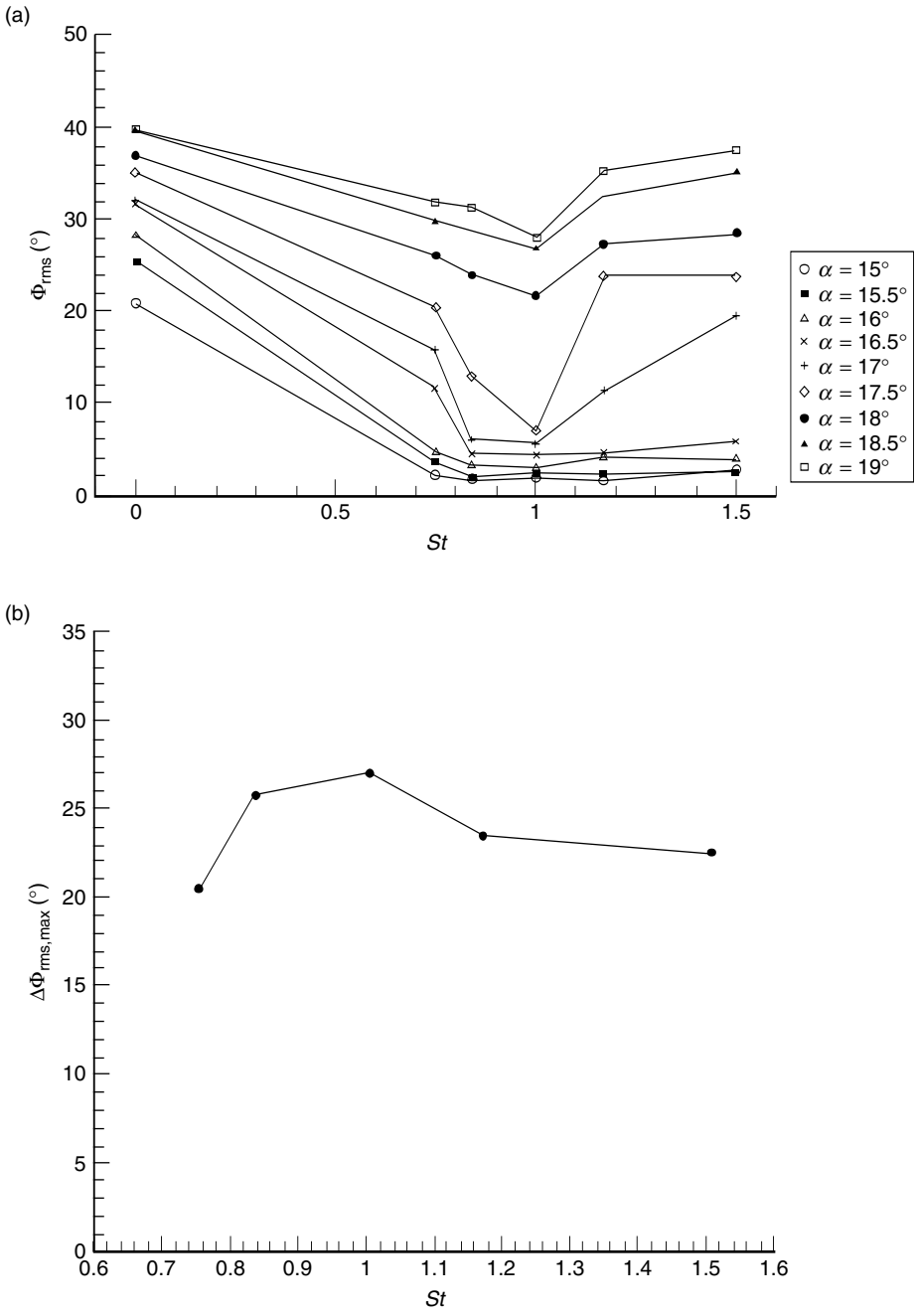

Figure 8. (a) RMS values of wing roll angle as a function of Strouhal number of synthetic jet excitation; (b) Maximum reduction of RMS values of the wing roll angle as a function of Strouhal number of synthetic jet excitation.

exhibits a local maximum at around $St = 1$, suggesting the optimum synthetic jet excitation frequency of $St = 1$. Figures 7 and 8 also show that, at the optimum excitation frequency of $St = 1$, the maximum values of RMS roll angle suppression, $\Delta\Phi_{rms,max}$ of about 27° was achieved at $\alpha = 17.5°$ (see Figure 7b). As the effectiveness of the excitation of the flow vanishes at large angles of attack, we find an optimal angle of attack of $\alpha = 17.5°$. Furthermore, as discussed earlier, the maximum delay by approximately $\Delta\alpha_{max} = 3.5°$ in the onset of the self-excited roll oscillations was achieved at $St = 1$ (Figures 5 and 7). Particle Image Velocimetry (PIV) flow measurements were conducted on the model to understand the underlying flow physics.

3.3. High Frame PIV measurements

A previous study [19] suggested that the shear layer separated from the leading-edge could be energized by acoustic forcing at an optimal frequency resulting in local reattachment or smaller separated region closer to the wing surface, thus attenuating the roll oscillations. Acoustic forcing is a global flow control approach, thus both the tip vortex and the shear layer separated from the leading-edge were excited at the same time. Present results suggest that the application of a local excitation at $St = 1$ is highly effective in attenuating self-induced roll oscillations. In this study, high frame rate PIV measurements were conducted over the stationary wing at $\Phi = 0°$ and $\alpha = 17°$ without and with synthetic jet excitation at $St = 1$.

Figure 9 shows the time-averaged velocity magnitude, streamline patterns and velocity power spectra near the leading-edge of the stationary flat-plate wing and in the streamwise plane at $y/(b/2) = 0$ (wing symmetry plane) for $\alpha = 17°$ and $\alpha = 0°$. (Some limited data at another spanwise plane ($y = b/4$) are available, however do not show any additional insight. Measurements at various spanwise planes are presented in elsewhere [18, 19], which show fully separated flow in other planes of the three-dimensional flow). There were several reasons for choosing the stationary wing for the time-accurate PIV measurements: (i) previous measurements at the symmetry plane [18, 19] did not show noticeable differences between the stationary wing and rolling wing at *zero roll angle*; (ii) time-accurate measurements for the rolling wing is not possible as the wing will block the illumination plane; (iii) instantaneous roll angle is close to zero for the free-to-roll wing when the excitation is applied.

For each case, frequency spectra of the streamwise velocity fluctuations were calculated from the PIV data near the shear layer at the locations of $x/c = 0.25$ and 0.5, which are denoted by symbol '+' in Figure 9. In the absence of flow excitation, the flow is fully separated at $y/(b/2) = 0$ (Figure 9a), which is consistent with previous studies [12, 19]. When the synthetic jet excitation at $St = 1$ is applied, the separated flow moves closer to the wing surface, the recirculation region becomes smaller and its centre seen in the time-averaged streamline pattern moves upstream towards the leading-edge. At $y/(b/2) = 0$ and $x/c = 0.25$, the frequency spectra of the "no synthetic jet excitation case" exhibits a small peak at around $fc/U_\infty \approx 1$, which becomes stronger at $x/c = 0.5$ (Figure 9b and c). It is believed that this peak corresponds to the dominant frequency of the shear-layer instabilities. With synthetic jet excitation at $St = 1$, both velocity spectra at $x/c = 0.25$ and 0.5 exhibit a sharp, more prominent peak at around $fc/U_\infty \approx 1$, suggesting a strong resonance between the synthetic jet excitation and the shear layer instabilities. Note that, at $x/c = 0.25$, the frequency spectra of the case with synthetic jet excitation exhibits a dominant peak at around $fc/U_\infty \approx 2$ as well, which corresponds to the harmonic of the excitation frequency.

Previous studies indicate that large amplitude self-excited roll oscillations of low aspect ratio flat-plate wings occur when the flow is fully separated from the wing surface at higher wing incidences [12]. Therefore, the aforementioned strong resonance at $St = 1$ energizes the shear layer separated from the leading edge and results in a local flow field that is more characteristic of a lower incidence (Figure 9a), which attenuates the roll oscillations. Figure 10 presents the time-averaged vorticity patterns over the stationary flat plate wing at $y/(b/2) = 0$, $\alpha = 17°$ and $\Phi = 0°$. It is noted that, with synthetic jet excitation at $St = 1$, the separating shear layer from leading edge is getting closer to the wing suction surface. This observation is more obvious by comparing the line of the maximum vorticity, which is superimposed on the streamwise velocity vectors in Figure 10, without and with the synthetic jet excitation. Figure 10c shows the velocity standard deviation corresponding to the velocity fields illustrated in Figures 10a and b. It can be seen that, with synthetic jet excitation, the region of strong

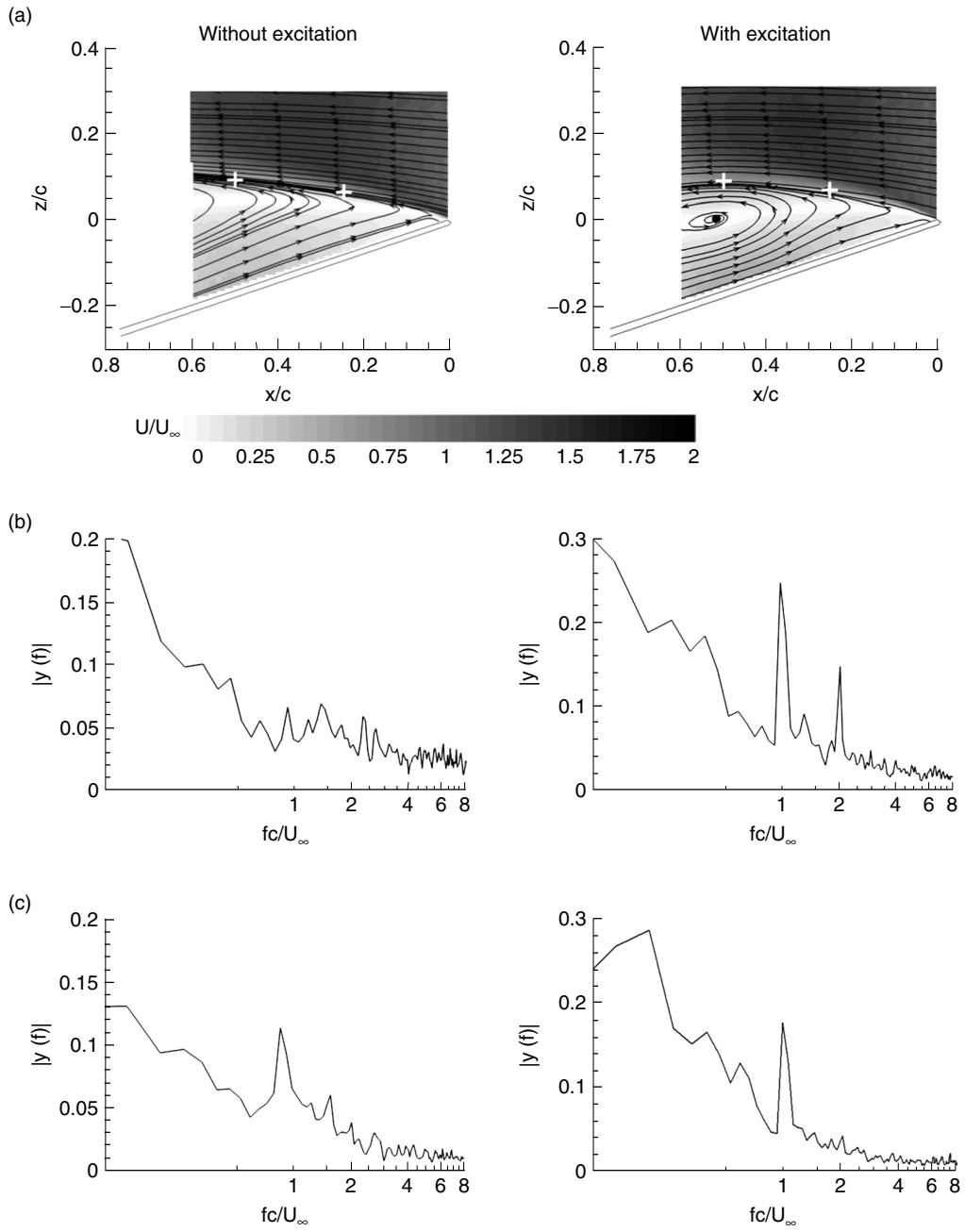

Figure 9. High frame-rate PIV measurements of velocity magnitude, streamlines and velocity power spectra over the stationary wing at spanwise locations of $y/(b/2) = 0$, $\alpha = 17°$ and $\Phi = 0°$ without and with synthetic jet excitation at $St = 1$; (a) velocity magnitude and streamlines; (b) velocity power spectra measured near the shear layer at streamwise location of $x/c = 0.25$; (c) velocity power spectra measured near the shear layer at streamwise location of $x/c = 0.5$.

velocity fluctuations becomes larger and closer to the wing suction surface and the fluctuation amplitude increases, suggesting intensified shear layer unsteadiness due to the resonance between synthetic jet excitation and shear layer instabilities. Effectively, this results in the local flow becoming closer to the wing surface as it would do at a smaller angle of attack, and thus supresses the self-excited roll oscillations.

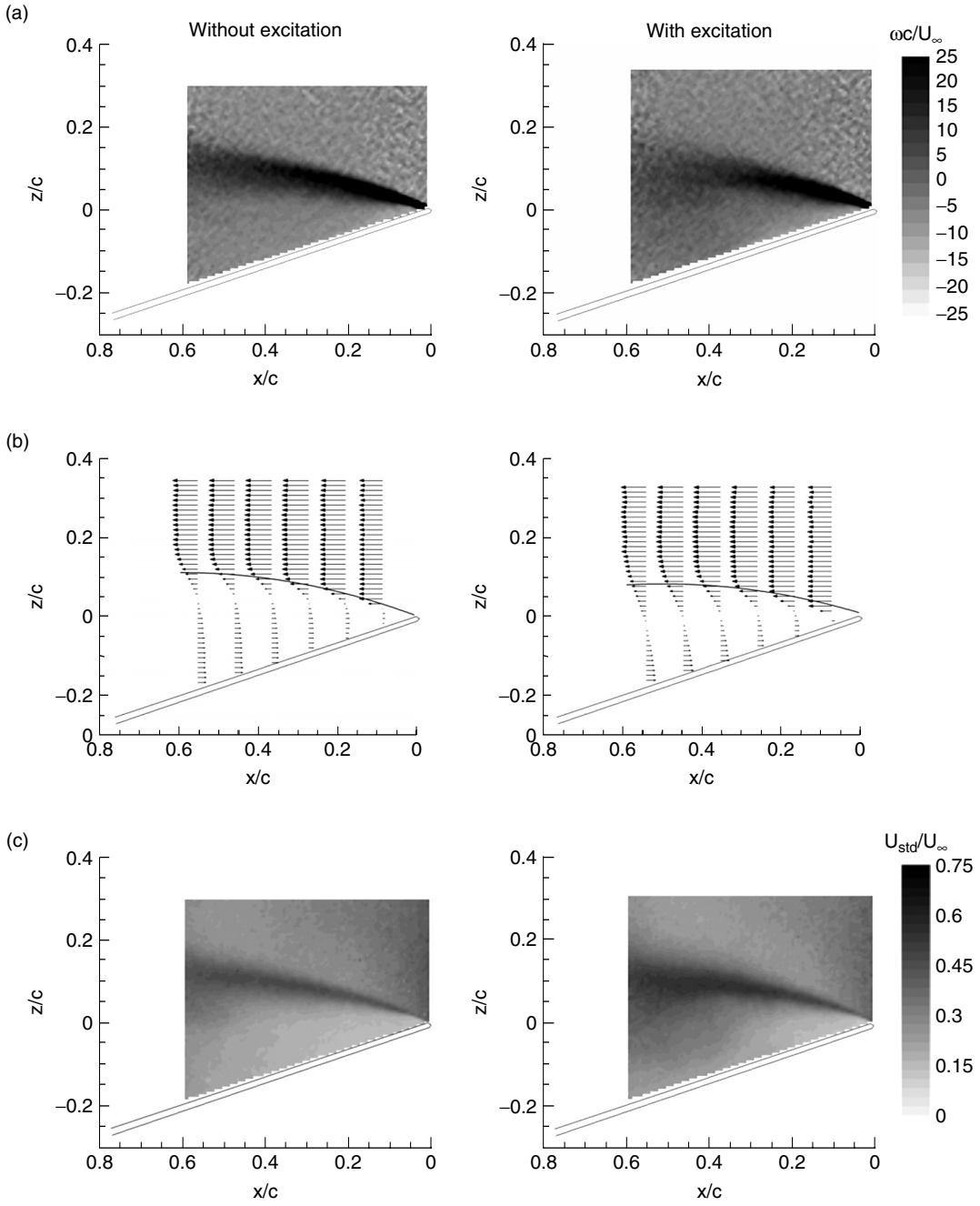

Figure 10. High frame-rate PIV measurements of (a) vorticity, (b) velocity profiles and (c) standard deviation of velocity over the stationary wing at $y/(b/2) = 0$, $\Phi = 17°$ and $\alpha = 0°$ without and with synthetic jet excitation at $St = 1$.

4. CONCLUSIONS

The effectiveness of synthetic jet excitation in suppressing large amplitude self-excited roll oscillations of a free-to-roll low aspect ratio flat-plate wing was investigated in wind tunnel experiments. The time histories of roll angle of the free-to-roll flat plate wing without and with synthetic jet excitation near the leading edge showed that, without synthetic jet excitation, the roll oscillations first appeared at a pre-stall incidence and the amplitude increased with increasing angle of attack. The roll oscillations can be effectively supressed by activating the synthetic jet excitation and its effectiveness on the roll reduction was closely related to the unsteady forcing frequency. At the optimum excitation frequency of $St = 1$, the maximum roll amplitude reduction of $\Delta\Phi_{rms,max} \approx 27°$ was achieved at $\alpha = 17.5°$ and the

onset of the roll oscillation was delayed by approximately $\Delta\alpha_{max} = 3.5°$. This is possible for very small values of momentum coefficient, on the order of $C_\mu = O(10^{-5})$.

The onset of large amplitude roll oscillations of the free-to-roll flat plate wing occurs with increasing angle of attack, and is related to the fully separated flow from the leading-edge. With synthetic jet excitation at the optimum frequency of $St = 1$, time-accurate high frame rate PIV measurements over the stationary flat plate wing at $\Phi = 0°$ and $\alpha = 17°$ in the streamwise plane at $y/(b/2) = 0$ (mid-span) revealed a strong resonance between the synthetic jet excitation and the shear layer instabilities. The resonance energizes the shear layer separated from the leading edge and results in smaller separated regions. Therefore, this effectively generates a local flow field that is more characteristic of a lower angle of attack, thus attenuating the roll oscillations.

ACKNOWLEDGMENTS

This work was supported by the RCUK Academic Fellowship in Unmanned Air Vehicles. The authors would like to thank the EPSRC Engineering Instrument Pool.

NOMENCLATURE

b	=	wing span
c	=	wing chord
d	=	thickness of the wing
E	=	Young's Modulus
f	=	frequency
I_{xx}	=	moment of inertia about x-axis
l	=	synthetic jet slot length
q_∞	=	freestream dynamic pressure, $\frac{1}{2}\rho U_\infty^2$
Re	=	Reynolds number, $\rho U_\infty c/\mu$
St	=	Strouhal number, fc/U_∞
t	=	time
U	=	streamwise velocity
U_j	=	synthetic jet velocity
U_∞	=	freestream velocity
w	=	synthetic jet slot width
x	=	chordwise coordinate
y	=	spanwise coordinate
z	=	distance from the wing surface in a direction normal to the freestream
α	=	wing angle of attack
μ	=	viscosity
ρ	=	density
ω	=	vorticity
Φ	=	roll angle
Λ	=	wing sweep angle
AR	=	aspect ratio
FFT	=	fast Fourier transform
LAR	=	low aspect ratio
MAV	=	micro air vehicle
PIV	=	particle image velocimetry
rms	=	root-mean-square
$\|Y(f)\|$	=	power spectral density of velocity fluctuations

REFERENCES

[1] Pelletier, A. and Mueller, T. J., Low Reynolds Number Aerodynamics of Low-Aspect-Ratio, Thin/Flat/Cambered-Plate Wings, *Journal of Aircraft*, 2000, 37(5), 825–832.

[2] Torres, G. E. and Mueller, T. J., Low-Aspect-Ratio Wing Aerodynamics at Low Reynolds Numbers, *AIAA Journal*, 2004, 42(5), 865–873.

[3] Krashanitsa, R., Platanitis, G., Silin, D. and Shkarayev, S., Autopilot Integration into Micro Air Vehicles, in *Introduction to the Design of Fixed-Wing Micro Air Vehicles* edited by Mueller, Kellogg, Ifju, Shkarayev. Published by the AIAA, 2007.

[4] Mueller, T., *Fixed and Flapping Wing Aerodynamics for Micro Air Vehicle Applications*, Published by the AIAA, 2001.

[5] Arena, A. S. J. and Nelson, R. C., Experimental Investigation on Limit Cycle Wing Rock of Slender Wings, *Journal of Aircraft*, 1994, 31(5), 1148–1155.

[6] Katz, J., Wing/Vortex Interactions and Wing Rock, *Progress in Aerospace Sciences*, 1999, 35, 727–750.

[7] Levin, D. and Katz, J., Self-Induced Roll Oscillations of Low-Aspect-Ratio Rectangular Wings, *Journal of Aircraft*, 1992, 29(4), 698–702.

[8] Williams, D. L. and Nelson, R. C., Fluid-Dynamic Mechanisms Leading to the Self-Induced Oscillations of LAR Wings, AIAA 97-0830, *35th Aerospace Sciences Meeting & Exhibit*, January 6–9, 1997, Reno, NV.

[9] Gursul, I., Gordnier, R. and Visbal, M., Unsteady Aerodynamics of Nonslender Delta Wings, *Progress in Aerospace Sciences*, 2005, 41, 515–557.

[10] Gresham, N. T., Wang, Z. and Gursul, I., Vortex Dynamics of Free-to-Roll Slender and Nonslender Delta Wings, *Journal of Aircraft*, 2010, 47(1), 292–302.

[11] Gresham, N. T., Wang, Z. and Gursul, I., Self-Induced Roll Oscillation of Non-slender Wings, *AIAA Journal*, 2009, 47(3), 481–483.

[12] Gresham, N. T., Wang, Z. and Gursul, I., Low Reynolds Number Aerodynamics of Free-to-Roll Low Aspect Ratio Wings, *Experiments in Fluids*, 2010, 49, 11–25.

[13] Mabey, D. G., Similitude Relations for Buffet and Wing Rock on Delta Wings, *Progress in Aerospace Sciences*, 1997, 33, 481–511.

[14] Katz, J. and Walton, J., Reduction of Wing Rock Amplitudes Using Leading-Edge Vortex Manipulations, AIAA 92-0279, 30th *Aerospace Sciences Meeting & Exhibit*, January 6–9, 1992, Reno, NV.

[15] Katz, J. and Walton, J., Application of Leading-Edge Vortex Manipulations to Reduce Wing Rock Amplitudes, *Journal of Aircraft*, 1993, 30(4), 555–557.

[16] Wong, G. S., Rock, S. M., Wood, N. J. and Roberts, L., Active Control of Wing Rock Using Tangential Leading-Edge Blowing, *Journal of Aircraft*, 1994, 31(3), 659–665.

[17] Sreenatha, A. G. and Ong, T. K., Wing Rock Suppression Using Recessed Angle Spanwise Blowing, *Journal of Aircraft*, 2002, 39(5), 900–903.

[18] Hu, T., Wang, Z. and Gursul, I., Control of Self-Excited Roll Oscillations of Low-Aspect-Ratio Wings Using Acoustic Excitation, 49th *AIAA Aerospace Sciences Meeting Including The New Horizons Forum and Aerospace Exposition*, Orlando, Florida, 4-7 January, 2011, AIAA-2011–36.

[19] Hu, T., Wang, Z. and Gursul, I., Attenuation of Self-excited Roll Oscillation of Low-Aspect-Ratio Wings by means of Acoustic Forcing, *AIAA Journal*, 2013, in print.

[20] Smith, B. L. and Glezer, A., The formation and evolution of synthetic jets, *Physics of Fluids*, 1998, 10(9), 2281–2297.

[21] Seifert, A., Darabi, A., and Wyganski, I., Delay of Airfoil Stall by Periodic Excitation, *Journal of Aircraft*, 1996, 33(4), 691–698.

[22] Greenblatt, D. and Wygnanski, I. J., The Control of Flow Separation by Periodic Excitation, *Progress in Aerospace Sciences*, 2000, 36, 487–545.

[23] Amitay, M. and Glezer, A., Role of Actuation Frequency in Controlled Flow Reattachement over a Stalled Airfoil, *AIAA Journal*, 2002, 40(2), 209–216.

[24] Glezer, A., Amitay, M. and Honohan, A. M., Aspects of Low- and High- Frequency Actuation for Aerodynamic Control, *AIAA Journal*, 2002, 43(7), 1501–1511.

[25] Whitehead, J. and Gursul, I., Interaction of Synthetic Jet Propulsion with Airfoil Aerodynamics at Low Reynolds Numbers, *AIAA Journal*, 2006, 44(8), 1753–1766.

[26] Margaris, P. and Gursul, I., Wing Tip Vortex Control Using Synthetic Jets, *The Aeronautical Journal*, 2006, 110(1112), 673–681.

[27] Mueller, T. and DeLaurier, J.D., An Overview of Micro Air Vehicles Aerodynamics, *Fixed and Flapping Wing Aerodynamics for Micro Air vehicle Applications*, edited by T.J. Mueller, vol. 195, Progress in Astronautics and Aeronautics, AIAA, Virginia, 2001, pp. 1–9.